# HUMAN SPINAL CORD ORGANOIDS REVEAL CELL INTERCALATION AS A CONSERVED MECHANISM FOR SECONDARY NEURULATION

**José Blanco-Ameijeiras[1], Mar García-Valero[1], Yara El Majzoub[1], Elena Rebollo[2], Javier Macho-Rendón[3], Jorge Corbacho[3], Juan Ramón Martínez-Morales[3] and Elisa Martí[1#]**

1.- Cells and Tissues Dept, Instituto de Biología Molecular de Barcelona, CSIC; Parc Científic de Barcelona, Baldiri i Reixac 20, Barcelona 08028, Spain.

2.- MIP, Instituto de Biología Molecular de Barcelona, CSIC, Parc Científic de Barcelona, Baldiri i Reixac 20, Barcelona 08028, Spain.

3.- Centro Andaluz de Biología del Desarrollo (CSIC/UPO/JA). 41013 Sevilla, Spain.

#- Corresponding author and Lead Contac

**Keywords:** spinal cord development; secondary neurulation; human organoids; YAP signalling; neural tube defects

**Word count 5442**

**INCLUSION AND DIVERSITY**

We support inclusive, diverse, and equitable conduct of research

## SUMMARY

The spinal cord originates from bipotent stem cells called neuromesodermal progenitors, which are organized in a transient embryonic structure called the neural tube. The development of neural organoids is offering unprecedented tools to advance in the limited understanding of the initial construction and subsequent maturation of the human neural tube. In this study, we have generated human neural tube organoids with defined anterior and posterior identities. Through transcriptome profiling, we identified that the posterior organoids possessed a spinal cord identity. By modifying the culture conditions, we recapitulated the morphogenetic events for secondary neurulation in vivo, and revealed that de novo lumen formation in the spinal cord organoids involves a conserved Yap-dependent cell intercalation process. We believe that these findings will contribute to our understanding of the mechanisms required for building the human spinal cord in the embryo, and to understand the biological basis of neurodevelopmental disorders, which are among the most common birth defects.


## INTRODUCTION

The spinal cord processes information from peripheral sensory neurons and manages motor responses by controlling neurons that innervate muscles. These activities are executed by neural circuits made up of molecularly unique neuronal subtypes, which are produced in a specific spatiotemporal order in the embryonic transient structure called the neural tube (NT). Based on the use of animal models, this transient NT has two different embryonic origins along its anterior-posterior axis; the brain is generated through neural induction of ectodermal cells, while the spinal cord arises from bipotent stem cells called neuromesodermal progenitors (NMPs), which are produced during body axis elongation ([1–4]). Regardless of this differential origin along the anterior to posterior axis of the NT, these cells self-organize into a continuous and transient hollow tube. Moreover, the 3D tissue rearrangements required for building the future spinal cord, along its anterior-posterior axis are different; the anterior spinal cord is organized through primary neurulation, while the posterior through secondary neurulation [5].

Morphogenesis of the posterior spinal cord is known as secondary neurulation, and it is a conserved process that can be followed at the elongating tailbud of the 25 somites in the chick embryos, at comparable axial levels of the mouse embryos (forming 30 somites), and in the human embryo (forming 25-30 somites; CS 12-14; week 5 post-fertilization) [6–10]. The transition along the antero-posterior axis between primary and secondary neurulation might vary among vertebrates, although probably takes place near to the site of final closure of the caudal neuropore. In the developing human spinal cord, only fragmented knowledge generated by the analysis of histological sections from human embryos from termination of pregnancies, is available. A structure resembling the medullary cord (the immediate precursor of the secondary NT) is observed at the site of the caudal neuropore. Moreover, multiple cavities are frequently observed in the medullary cord of the human embryo tailbud [6–9] closely resembling the multilumen transitional process that described for SNT formation in the chick embryo [10]. Regardless of the conservation and relevance of this process for building a functional spinal cord, descriptive and functional studies are infrequent in animal models and in humans limited to the availability of these samples. This lack of current knowledge is holding back understanding the etiology of those defects that compromise the formation of the posterior spinal cord, are compatible with life, and are the most frequent structural birth defect of the central nervous system, globally termed neural tube defects (NTD) [11,12].

Today the development of human neural organoids is offering unprecedented tools to study the mechanisms required for building the human nervous system in health, and to understand the biological basis of neurodevelopmental disorders. These technologies use human pluripotent stem cells guided to the development of specific cell identities by manipulating signaling factors that, together with the use of 3D substrates, allow for the self-organization of multicellular regions of the embryo, the so-called organoids [13,14]. Among the available organoids mimicking several traits of NT development [15–23], reliable human posterior spinal cord organoids were still to be developed.

To fill this knowledge gap, here we set to generate human spinal cord organoids, by exposing pluripotent stem cells (PSCs) to various extrinsic signals which play crucial roles in controlling the temporal and spatial regulation of gene expression necessary for building the NT along the anterior-to-posterior embryo axis [24,25]. Our screening strategy demonstrated that the self-assembling properties of PSC can be directed to generate

organoids to mimic the developmental time window and the correct anterior posterior axis identity of the human secondary NT (SNT).

Moreover, to investigate the tissue dynamics of secondary neurulation, we refined our engineered in vitro system to more closely mimic the in vivo process. In our posterior organoid model of secondary neurulation, we demonstrated that cell intercalation, regulated by the activity of Yes-associated protein (YAP), acts as a key morphogenetic mechanism for lumen formation. This indicates a conserved mechanism, similar to that observed in chick embryos [10]. Collectively, these findings establish the first human organoids with a posterior spinal cord transcriptional identity and provide a reliable model of secondary neurulation, which may advance our understanding of the biological basis of neural tube defects (NTDs).

## RESULTS

### Generation of human neural tube organoids with different anterior-posterior identities

During neural tube (NT) formation, progenitor cells are sequentially exposed to a variety of extrinsic signals, including members of the TGFβ/BMP, WNT, FGF and RA signalling families (Figure 1A). These signals play crucial roles in controlling the temporal and spatial regulation of gene expression, which in turn regulates lineage restriction and the generation of specific cell identities necessary for building a functional nervous system [26–29]. Here we have set to mimic the embryo environment to guide human pluripotent stem cells to build neural tube (NT) organoids.

Members of the TGFβ/BMP signalling pathway are known to be present and active during neural induction and neural plate formation [29]. *In vitro* studies conducted in both 2D [30,31] and 3D cultures [19,32] have reported that double inhibition of TGFβ and BMP leads to rapid neural conversion. We initially seeded human embryonic stem cells (hESC; RUES2) on matrigel and cultured them in neural induction medium (N2B27) with transient inhibition of BMP and TGFβ signalling (48-hour treatment with the BMP type I receptor ALK1-3 inhibitor LDN193189, and the TGFβ type I receptor ALK4,5,7 inhibitor SB431542). This resulted in the organization of multicellular cysts, termed neural organoids, consistently

composed of SOX2+ cells (Figure 1B, C). Concomitantly with the neural lineage restriction of hESCs, these SOX2+ cells underwent epithelialization, as evidenced by the apical localization of aPKC, and self-organized around a single central lumen (Figure 1C). These 48-hour pulse of TGFβ/BMP inhibition was mimicking neural induction and the formation of the anterior neural identity, as reported [19,32]

Our aim was to establish a combination of extrinsic signals that closely mimics the environment of the elongating embryo, and hence the spinal cord formation (Figure 1A). This combination should effectively guide the conversion of NMP cells, as monitored by the dynamic expression of SOX2/BRA, and consecutively promote the mesenchymal-to-epithelial transition and the self-organization around a single lumen. To begin to mimic the signalling environment of the posterior embryo, we exposed the hESC to the WNT agonist CHIR (CHIR99021) for 24 hours, followed by a 48-hour supplementation of CHIR along with basic FGF (bFGF) [33,34]. Consistent with previous studies in mouse ES cells and mouse epiblast cells [35], this resulted in the presence of BRA, which is a target of WNT and FGF [36], however was insufficient for neural induction, as indicated by the absence of SOX2 expression. Moreover, this condition appeared to be insufficient to guide neural progenitor conversion, reflected by the failure of complete a MET and the failure to organize a central lumen (Figure 1 B; Supplementary Figure 1A,B).

Next, we exposed hESCs to WNT/bFGF along with TGFβ and/or BMP inhibition, to burst neural induction. Results showed that, in the presence of WNT/bFGF, neither BMP inhibition alone, nor the double TGFβ/BMP inhibition, were sufficient to promote the neural identity, as reflected by the low percentage of organoids containing SOX2+ cells (Figure 1B; Supplementary Figure 1A, C, D).

In the elongating embryo, Retinoic Acid (RA) mainly secreted from the somites (Figure 1A) plays an instructive role by opposing WNT activity and regulating the balance between the NMP cell fate and neural identity[3,37] .To mimic this embryonic environment, we exposed hESCs to neural induction medium supplemented with WNT/bFGF, BMP inhibition, and RA for 48 hours. After three days of this treatment, hESCs efficiently formed small organoids consisting of NMP-resembling cells expressing SOX2/BRA (Figure 1 B, C). The temporal evolution of these NT organoids also resembled the lineage

restriction of NMP cells *in vivo*, with the presence of SOX2+ cells gradually increasing, while the presence of BRA+ cells decreased. Furthermore, these organoids efficiently self-organized to form a single central lumen (Figure 1 B, D). We next tested whether BMP inhibition was dispensable for the formation of these NT organoids. After three days of growing hESCs in medium supplemented with WNT/bFGF and RA for 48 hours, organoids were formed where the presence of BRA+ cells was consistent, while that of SOX2+ cells was irregular (Figure 1 B; Supplementary Figure 1 A, E), altogether indicating the relevance of TGFβ/BMP inhibition for an efficient neural induction.

Next, to investigate whether the caudal limit observed in mouse ESC differentiation without WNT signalling is conserved in human cells, we examined organoids generated from hESCs cultured under conditions that inhibited TGFβ/BMP activity. In these organoids, the presence of CDX2+ cells was rare, indicating an anterior identity of these organoids (Figure 1B and C). However, when hESCs were cultured in the presence of WNT/bFGF, BMP inhibition, and RA, organoids consistently and robustly exhibited the presence of CDX2+ cells, indicative of a posterior NT identity (Figure 1B and D). This suggests that WNT signalling has the capacity to directly activate CDX2 expression, which in the elongating embryo plays a crucial role in ensuring spinal cord identity by repressing regional hindbrain identity of the neural tissue [38]. Altogether, these findings indicate the spinal cord (posterior) identity of these organoids.

Finally, to demonstrate the robustness of NT organoid formation, we utilized induced pluripotent stem cell (human iPSC) lines, namely Kolf2-C1 and CRTD1. We cultured these iPSCs in neural induction medium with different conditions to guide the generation of organoids with distinct anterior and posterior identities. When iPSCs were cultured with transient inhibition of TGFβ/BMP signalling for 48h, they were directed to form NT organoids with anterior neural identity. On the other hand, when iPSCs were cultured in neural induction medium supplemented with WNT/bFGF, BMP inhibition, and RA, they were guided to form NT organoids with spinal cord identity (Supplementary Figure 2). These findings demonstrate that the self-assembling properties of human pluripotent stem cells can be directed to generate NT organoids with defined anterior and posterior identities.

**Transcriptome profiling of NT organoids revealed different anterior and posterior neural identities**

To define the identity of the *in vitro*-generated NT organoids, we performed bulk RNA sequencing (RNA-seq) using three biological replicates of anterior (A) and three replicates of posterior (P) NT organoids (Figure 2A). These organoids were generated from human embryonic stem cells (hESC; RUES2) and were grown *in vitro* for 6 days. During this culture period, the organoids acquired the A and P identities, respectively, but neurogenesis was not initiated. We employed the DNASEQ platform from BGI to identify 17,462 genes, with an average mapping ratio to the reference genome of 98.03% (Reference Genome Version: GCF_000001405.39_GRCh38.p13). The Pearson correlation coefficients between samples revealed low gene expression variability among the three A and the three P organoid samples (Figure 2B). A total of 8,728 differentially expressed genes (DEGs) were identified when comparing the transcriptomes of the A and P organoids (Figure 2C). By examining the gene expression profiles of key neural, mesodermal, and endodermal markers we confirmed the neural characteristics of the NT organoids (Supplementary Figure 3 A,B).

To gain further insight into the anterior to posterior identity of the NT organoids, we compared our samples with single-cell RNA-sequencing data from samples of forebrain, midbrain, hindbrain and spinal cord from human embryos at Carnegie stage 14, (corresponding to the week 5 of development), a developmental stage comparable to mouse embryo day 10, in which neurogenesis in the spinal cord is only initiated ([39]). Attempts to use standard unsupervised methods to cluster the organoids transcriptome data were unsuccessful at classifying them into the reported anterior to posterior embryo data (forebrain, midbrain, hindbrain and spinal cord). Hence, to refine the characterization of the A and P organoids, we examined the expression levels of a diagnostic panel of 41 genes, that are specifically expressed along the A-P axis of the developing CNS at distinct domains [40–49]. Through comparative principal component analysis of all samples, we observed that the A organoid samples clustered together with the anterior nervous system, including CS14 forebrain, midbrain, and hindbrain controls, while the P organoid samples were closer to the CS14 spinal cord control (Figure 2 D). By employing a hierarchical clustering approach, we gained further insights into the identity of A and P NT organoids (Figure 2 E). The anterior organoids exhibited similarity with forebrain samples, with the notable absence of a group of genes expressed in the dorsal telencephalon and neural

retina domains, such as *EMX2*, *RAX2*, *FOXG1*, *LHX2*, *FEZF2*, and *DLX2*. This finding, in conjunction with the principal component analysis, suggested that our culturing conditions did not favour the *in vitro* specification of the precursors towards dorsal retina and forebrain identities. Instead, they directed them towards ventral midbrain and retinal (i.e., optic stalk) derivatives, as indicated by the expression of genes like *VAX1*, *SIX6*, *SIX3*, or *FEZF1*. However, the gene expression of A organoids showed the highest similarity with midbrain-hindbrain CS14 samples (Figure 2 E)

On the contrary, the gene expression clustering of P organoids samples revealed the remarkable absence of brain-specific gene expression, while these neural progenitors are capable of generating a full range of anterior-posterior spinal cord derivatives (Figure 2 E). As such, the P organoids expressed both anterior (e.g., *HOX2-4*) and posterior *HOX* (e.g., *HOX12-13*) spinal cord genes, as well as very distal markers such as *CDX2* or *EFNA2*. Importantly, to our knowledge these are the first NT organoids exhibiting a robust spinal cord transcriptome identity, including the most posterior spinal cord, at the regions were the NT is developed through the morphogenetic process called secondary neurulation (SN)[5].

Finally, we assessed the dorso-ventral (DV) identity of the posterior NT organoids by examining a diagnostic panel of 35 DV markers [50,39] (Supplementary Figure 3 C). This analysis revealed that in contrast to the CS14 spinal cord controls, which expressed a full range of DV markers, posterior NT organoids have a dorsal identity, with most ventral genes (e.g. *SHH*, *NKX2.2*, or *OLIG2*) being almost absent (Supplementary Figure 3 D).

**NT organoids are organized by cells exhibiting cell architecture and dynamics resembling those of the neural progenitor cells.**

Regardless of the differential origin along the anterior to posterior axis of the NT, the architecture of the early embryonic NT (midbrain/hindbrain and spinal cord) is conserved along its entire A P axis, consisting on a hollow tube built by highly polarized neural progenitor cells (NPCs). We next set to evaluate whether the cellular and subcellular organization of A and P human NT organoids, mimic the embryonic NT cell architecture and dynamics.

During NT formation in the chick and mouse embryo NPCs elongate [51]. Hence, we first compared the cell shape of hESCs cultured in the presence of WNT/bFGF (resulting in a mesenchyme-like tissue organization) to those cultured in neural induction medium guided for either A or P identities. The results demonstrated a significant elongation of NPCs, in both A and P organoids. The major axis/minor axis ratio of the cell shape was increased in NPCs of A organoids (Figure 3A and C median ± IQR major axis/minor axis = 3.88 ± 1.97) and P organoids (Figure 3 B and C median ± IQR major axis/minor axis = 4.37 ± 1.71) compared to mesenchymal cells in WNT/bFGF conditions (Supplementary Figure 4 B, Figure 3 C median ± IQR major axis/minor axis = 1.48 ± 0.48)

During NPCs elongation, the perinuclear centrosome relocates apically, as indicated by its alignment with N-Cadherin expression along the NT lumen. En face imaging of organoids revealed the localization of N-Cadherin to the NPC apical belt and the central localization of Pericentrin (PCNT+)-labelled centrosomes (Figure 3 D, E). Quantification of the distance between the PCNT+ labelled centrosomes and the nucleus showed their apical localization in elongated NPCs of both in both A and P organoids (median ±IQR distance mesenchymal cells = 1.46 ±0.63 μm vs A organoids NPCs = 10.18 ±11.54 μm, and A organoids NPCs = 7.21 ±7.55 μm, Figure 3 D-F). The distance of PCNT+ centrosomes from the nucleus exhibited wide variation, which could be attributed to the onset of interkinetic nuclear migration (INM), a process that separates or brings together the centrosome and the nucleus depending on the phase of the cell cycle, similar to what occurs in the developing NT *in vivo*. These findings indicate that our organoids display cellular and subcellular organization resembling that of the embryonic NT, including the elongation of NPCs and the apical localization of centrosomes in relation to the nucleus [51].

NPCs are characterized by the presence of a single primary cilium at their apical surface, which is nucleated by the basal body [52], and extends into the lumen of the NT in the developing embryo. In both A and P organoids, the lumen surface was found to be decorated with primary cilia, identified by the expression of the protein ADP-ribosylation factor-like 13b (ARL13B), which specifically associates with the ciliary membrane [53,54](Figure 3 G, H). The length and dynamics of these primary cilia in human NPCs generated *in vitro* were similar to those observed in the chick embryo NT [55] . The length

of Arl13b-labeled cilia protruding from the centrosome at the lumen of organoids was measured and showed comparable values (median ± IQR length: mesenchymal cells = 1.86 ± 0.98 µm, A organoids NPCs = 1.11 ± 1.03 µm, A and P organoids NPCs = 1.29 ± 0.92 µm, Figure 3 G-I). During cell division in organoids, ARL13B was observed to accumulate near one of the centrosomes that nucleated the mitotic spindle (Figure 3 G' and H'). This finding suggests that, similar to observations in the developing mouse neocortex [53] and the chick embryo NT [54], the primary cilia were not completely disassembled before mitosis. To further confirm the apical localization of the cilia, 3D reconstructions of the apical end foot of NPCs were generated, which revealed the presence of a single cilia pointing towards the lumen in organoids (Figure 3 G'' and H''). These observations demonstrate that A and P organoids exhibit the characteristic presence and localization of primary cilia, similar to the NPCs in the developing NT.

During NT formation, the apical membrane of NPCs undergoes reorganization into distinct micro-domains. In these micro-domains, specific proteins involved in junctional complexes (such as N-cadherin, α-catenin, and β-catenin) are located in the subapical domain, zonular proteins (including ZO1, afadin, and actin) occupy an intermediate position, and fate-determining factors (such as PAR3, aPKC, and prominin-1) are confined to the most external domain[56–59] .Transversal and *en face* imaging of organoids revealed the localization of N-Cadherin and β-Catenin at the apical belt of NPCs, resembling the distribution observed *in vivo* (Figure 3D', E', D'', E'', G" and H"). Furthermore, co-staining of aPKC and ZO1 demonstrated that NPCs within both A and P organoids organize membrane microdomains lining the lumen, closely resembling the organization seen in NPCs of the developing NT. In this arrangement, the aPKC microdomain faces the organoid lumen and is positioned external to the ZO1 membrane domain (Figure 3 J-K). These analyses collectively indicate that both A and P human organoids are composed of NPCs exhibiting a cell and tissue architecture highly similar to that of the embryonic NT.

To directly investigate the dynamics of neural progenitor cells (NPCs) within the human organoids we employed the piggyBac™ transposon system (pCAG-PBase) to electroporate hESCs with a GFP vector (PBCAG-eGFP). The GFP-expressing hESCs were cultured under conditions that guide the formation of mosaic P human organoids, which were then imaged using an Andor Dragonfly 505 confocal microscope. This

imaging system allowed organoids to grow at a similar rate as in normal culture conditions and enabled the segmentation and tracking of fluorescently labelled electroporated cells over time (Figure 3 M). Tracking the GFP+ cells allowed us to estimate the total cell cycle length within a span of 40 hours by measuring the time taken between cell shape changes, as well as the time taken for cells to transit from the organoid lumen to the basal end and back to the lumen (Figure 3 N and Supp. Movies S1, S2). Time-lapse imaging of human organoids revealed the stereotypic movement pattern of NPCs synchronized with the cell cycle, known as INM [60]. GFP+ cells in contact with the organoid ventricle displayed a high circularity associated with the rounded nucleus during mitosis (M) (Figure 3 O-Q and Supp. Movies S1, S2).Throughout the cell cycle, the nucleus of NPCs exhibited specific movements: during the G1 phase, the nucleus travelled basally, and the cell extended two feet contacting the apical and basal tissue limits; during the S phase, the nucleus contacted the basal region (periphery of the organoid); and during the G2 phase, the nucleus travelled apically toward the organoid lumen, while the cell extended two feet contacting the apical and basal regions (Figure 3 O-Q and Supp. Movies S1, S2). Additionally, cell tracking enabled the estimation of the duration of different cell cycle phases: G1 phase (median ±IQR time = 2.25 ±5.12 hours), S phase (median ±IQR time = 26.75 ±7 hours), G2 phase (median ±IQR time = 9.5 ±3.63 hours), and M phase (median ±IQR time = 1 ±0.38 hours) (Figure 3 N and Supp. Movies S1, S2). Overall, these data demonstrated the robustness of the *in vitro* generated NT organoids, not only in terms of transcriptional identity but also in terms of cellular architecture and dynamics. Consequently, these unique biomodels can be utilized to investigate the biological processes involved in posterior spinal cord development, which is poorly understood but crucial as abnormalities during this process can lead to neural tube defects, among the most common birth defects observed in humans[61].

**Modelling secondary neurulation in human spinal cord organoids**

Our current understanding of how the posterior spinal cord develops in human embryos is fragmentary [6–9], and it is largely based on studies in various vertebrate animal models. In the chick embryo, we have shown that the confinement of NMPs into the prospective medullary cord (which is the immediate precursor of the secondary neural tube, or SNT) is concomitant with the deposition of an extracellular matrix (ECM) containing classical cell-surface-associated glycoproteins [10]. As NMPs transform into fully epithelialized NPCs, multiple small lumens emerge *de novo* at the interface between the peripheral

epithelial and central mesenchymal cell populations. These small lumen foci appear at a distance equivalent to one cell's length from the developing basement membrane [10].

In line with this *in vivo* process, our study demonstrated that hESCs possess an intrinsic capacity to self-polarize and self-organize around a single central lumen. However, it should be noted that our culture conditions involve the clonal growth of small clusters of hESCs, where all the cells are in contact with a matrigel basement membrane-like environment. As a result, the forming organoids lack central cells with mesenchymal polarity (Figure 1 C, D). To better mimic the *in vivo* secondary neurulation cell rearrangements, we hypothesized that starting with a larger clump of hESCs would allow the presence of central cells isolated from the matrigel. Hence, we maintained GFP-expressing hESCs in agitation for 24 hours to form cell aggregates with mesenchymal features (Figure 4 A, B). After transferring these aggregates into 3D matrigel and culturing them in neural induction medium supplemented with WNT/bFGF, BMP inhibition, and RA, posterior NT organoids were formed. In these organoids, peripheral cells elongated and acquired epithelial polarity while central cells retained mesenchymal morphology, resembling the embryonic medullary cord (Figure 4 B). Importantly, under these culture conditions, de novo emergence of small lumen foci occurred at a distance equivalent to one cell's length from the matrigel. Over time, these small foci resolved into a single central lumen (Figure 4 A, B), closely resembling the morphogenetic events observed during posterior spinal cord development in both humans and chick embryos through secondary neurulation [6–10]. Notably, this capacity to organize a solid medullary cord and to open multilumens is restricted to the posterior NT organoids. Results show that hESC that were maintained in agitation for 24 hours to form cell aggregates with mesenchymal features, when guided to form anterior NT by a 48-hour pulse of TGFβ/BMP inhibition, rarely organize multiple lumens (Supplementary Figure 5A-F), indicating that this is a morphogenetic property associated to the posterior spinal cord organoids, as in the elongating embryo.

In the chick embryo posterior spinal cord, the resolution into a single lumen involves the intercalation of centrally located cells among the epithelialized NPCs, a process independent of apoptosis [10]. Our analysis of the human posterior NT organoids aimed to test the conservation of these mechanisms. We tracked the dynamics of GFP-expressing cells within the posterior NT organoids using time-lapse microscopy (Figure 4 C).

Observations of GFP+ cells revealed the presence of round mesenchymal cells located centrally within the organoids (indicated by a red asterisk and depicted in the initial time-points in Figure 4 D-F). Importantly, we consistently observed these central cells intercalating into the lateral walls of the neuroepithelium, resulting in a lateral movement away from the centre of the organoid (Figure 4 D; Supp. Movies S3-6). Notably, the intercalating cells exhibited a round shape and displayed high protrusiveness. The intercalation of these cells consistently led to cell elongation (Figure 4 E,F; Supp. Movies S3-6). These findings suggest that the intercalation of centrally located cells into the lateral walls of the neuroepithelium, resulting in cell elongation, is a conserved mechanism for the resolution into a single continuous lumen in the posterior human NT organoids, similar to what is observed in the chick embryo secondary neural tube formation. Importantly, this process does not involve apoptosis, as demonstrated by the absence of cleaved caspase-3 staining in the peripheral NPCs or the inner cells surrounded by forming lumens in the organoids (Supplementary Figure 5 G-I).

**Lumen resolution in posterior NT organoids involves YAP mediated cell intercalation**

In our investigation of the posterior NT organoids, we made an interesting observation regarding cell density during the process of cell intercalation. We found that the density of cells shifted from low in the central areas to high cell density in the peripheral NPCs; with cells occupying more space in the central region and being more compact in the peripheral (median ±IQR central cell area = 178 ±66,3 $\mu m^2$ vs peripheral cell area = 115 ±37,8 $\mu m^2$; Figure 5 A,B). Hippo effectors YAP/TAZ act as on-off mechanosensing switches by sensing modifications in extracellular matrix (ECM) composition and mechanics, as such, the increase in cell density is known to decrease the activity of the Hippo pathway, unleashing the nuclear shuttling of its downstream effector, YAP [62–65] (Figure 5 B).

To examine the role of YAP in the process of lumen resolution, we analyzed the endogenous YAP protein levels in the posterior human NT organoids during the clearance of central mesenchymal cells. Immunostaining for endogenous YAP revealed that active YAP (nuclear/cytoplasmic ratio) was higher in the central intercalating cells compared to the peripheral NPCs (median ± IQR ratio YAP nuclear/cytoplasm in central cells = 0,43 ±0,20 vs peripheral cells = 0,30 ±0,11; Figure 5 C and D). This finding is consistent with

recent reports on the morphogenetic process of lumen resolution in the chick embryo posterior spinal cord, where the higher YAP activity in the central cells indicates its involvement in regulating cell intercalation and lumen resolution [10].

To further investigate the requirement of YAP activity in cell intercalation and lumen resolution, we conducted experiments using dasatinib, a C-SRC/YAP1 inhibitor [66]. 3D image reconstruction of NT organoids showed that after 4 days in matrigel, the control organoids resolve a single central lumen, while dasatinib -treated organoids present a multilumen phenotype (Figure 6 A, B; Supp. Movies S7 and 8). Following the secondary neurulation morphogenic progression, we observed that control organoids after 3 days of culture in matrigel had already coalesced the lumen foci into a single central lumen (Figure 6 C, D; day 2 7/18, day3 21/21, day4 16/16). Conversely, the organoids treated with dasatinib were unable to resolve a single lumen and instead exhibited a multi-lumen phenotype even after 4 days of culture, resembling neural tube defects (Figure 6 E, F; day 2 1/8, day3 2/5, day4 4/18). This indicates the crucial role of YAP activity in the proper resolution of lumens and suggests that dysregulation of YAP signalling could contribute to neural tube defects such as spinal bifida.

These findings demonstrate that the posterior human NT organoids not only exhibit a transcriptome profile resembling the developing spinal cord of the early human embryo but also replicate cellular dynamics observed during the morphogenesis of the human embryo's secondary neural tube. This biomodel provides a unique platform to directly study the underlying mechanisms of neural tube defects such as spinal bifida.

## DISCUSSION

In this study, we successfully replicated the development of the posterior human spinal cord using *in vitro* techniques. We directed human pluripotent stem cells, including both embryonic stem cells and induced pluripotent stem cells, to differentiate into neural cells, specifically those with a spinal cord identity. By creating a culture environment that mimicked the conditions of the elongating embryo, we generated 3D organoids that exhibited a transcriptional profile indicative of spinal cord tissue. These spinal cord

organoids were composed of neuroepithelial cells that displayed a subcellular architecture similar to that of the embryonic NT. Numerous organoids have been developed that mimic several traits of NT development [1–4]; nonetheless, here we have generated a reliable human spinal cord organoid model, that reproduce the transcriptome identity of the early embryo spinal cord (5 weeks of development). Moreover, the cellular dynamics observed in the organoids also resembled the morphogenetic events involved in secondary neurulation, a process poorly understood, hence these models might bridge the knowledge gap regarding the formation of the human posterior spinal cord.

This understanding is crucial for elucidating the biological bases of neural tube defects (NTDs) which are frequent congenital disorders, thereby providing significant medical insights into primary prevention and reduce suffering caused by loss of movement in the legs, and bladder and bowel dysfunction, caused by NTDs such as spina bifida. NTDs in humans arise from a combination of genetic and environmental factors, classifying them as a multifactorial disorder [11,12]. Even though NTDs are the most frequent structural birth defect of the CNS, the causes remain mostly unknown. Heritability is estimated at 70%, and environmental factors that increase the risk include a lack of folic acid and maternal diabetes [12]. However, most genetic studies focused on single-nucleotide variants or small insertion / deletions for only affected individuals, studies showing that of the ~eleven loci mapped to date, eight encode core components of the planar cell polarity (PCP) pathway [67–70]. These genetic data, together with our experimental analysis in the chick embryo secondary neurulation, support the hypothesis that NTDs might arise from defects in the NMPC dynamics, such as a) the mesenchymal-to-epithelial transition of NMPCs required for full epithelialization of progenitor cells in building the caudal NT, and b) the tissue rearrangements required for the de novo lumen formation and single lumen resolution, to build a hollow NT. These are morphogenetic processes that are still to be revealed in human development, and the organoids engineered in this study holds promise for advancing our understanding of the biological bases and the tissue dynamics associated with secondary neurulation.

Our study conducted in chick embryos revealed the involvement of YAP/TAZ [10], which act as key sensors of cell density [71], in the intercalation of central cells during the resolution of the lumen in the secondary neural tube. Consistent with this model, human neural tube organoids generated in this study exhibited higher levels of nuclear (active)

YAP in the central cells compared to the peripheral neuroepithelial cells. Furthermore, when the Hippo pathway, which regulates YAP/TAZ activity, was blocked using the pharmacological inhibitor Dasatinib, the process of lumen resolution was impaired, resulting in a multilumen phenotype resembling NTDs. These findings support the idea that the YAP pathway mediates lumen resolution in response to cell density during secondary neurulation. While further research is necessary to fully understand the mechanisms underlying secondary neurulation and its association with NTDs, the results of this study lay the groundwork for generating patient-derived organoids. This approach holds promise for advancing our understanding of diseases associated with secondary neurulation and may contribute to the development of improved therapeutic strategies including the use of YAP/TAZ activators to alleviate some NTDs.

**Limitations of study**

In the study, we acknowledge the presence of inter-organoid variability in the generated organoids. While we observed reduced variability compared to longer protocols for organoid generation, we still noted some variability within the droplets and cell lines used. Specifically, a small proportion of organoids did not exhibit the expected lineage restriction. This variability should be considered when utilizing the model for pharmacological screenings, and further refinement of the protocols may be necessary to improve the consistency and reliability of the organoid system.

## ACKNOWLEDGMENTS

The authors are indebted to Leica Microsystems for supporting and collaborating with the MIP Platform (IBMB). We are grateful to researchers that kindly provided DNAs and antibodies, as indicated in the reporting summary. The work in EM's laboratory was supported by grants PID2022-139609NB-I00 and RED2022-134100-T. JBA is a recipient of a BES-2017-080050 PhD scholarship. The work in JRMM laboratory was supported by grants PID2020-112566GB-I00 and RED2022-134100-T. JMR is a recipient of a Juan de la Cierva 2022-AEI and JG of a PTA 2019-AEI

## AUTHOR CONTRIBUTIONS

**JBA** developed methodology, conceived and performed most of the experiments, analysed the data, discussed the results and revised the manuscript.

**MGV and YEM** performed a significant group of experiments, analysed the data, discussed the results and revised the manuscript.

**JMR, JC and JRMM** conceived the transcriptome profiling experiments, analysed and discussed the results, wrote those sections and revised the manuscript.

**EM** supervised the study, conceived the experiments, analysed the data, discussed the results and drafted the manuscript together with JRMM.

## DECLARATION OF INTERESTS

The authors declare no competing interests

## FIGURE LEGENDS

**Figure 1: Generation of NT organoids with different anterior-posterior identities (see also Figures S1-3).**

**(A)** Schematic representation of an embryo; the forming brain is shown in purple, the spinal cord in yellow and the somites are shown in green.

**(B)** Quantification of organoids expressing the indicated markers¸ SOX2 (red), BRA (green) and CDX2 (yellow), after 3, 5 and 7 days in culture. Guiding drugs are indicated at the appropriate days in culture. **(C)** Selected images of anterior NT organoids stained for SOX2 (red), BRA (green), aPKC (grey) and CDX2 (yellow) at day 3 **(C')**, day 5 **(C'')** and day 7 **(C''')**. **(D)** Selected images of posterior NT organoids stained for the indicated markers day 3 **(D')**, day 5 **(D'')** and day 7 **(D''')**. Scale bars = 30 µm.

**Figure 2: Anterior and Posterior NT organoids show different transcriptome identity. (A)** Schematic representation of organoid culture and RNA extraction for bulk RNA Sequencing. **(B)** Heatmap of the pairwise Pearson correlation coefficients of gene expression in the three replicates for both Anterior and Posterior organoids. **(C)** Volcano plot representation of differential expression analysis of genes in Posterior and Anterior NT organoids.

**(D)** Principal Component Analysis (PCA) of RNAseq-based expression data of selected genes for forebrain (purple), midbrain (lilac), hindbrain (purple) and spinal cord (mustard) samples isolated from CS14 human embryos and anterior (blue) and posterior (yellow) NT organoid samples.

**(E)** Schematic representation of an embryo; the Anterior forming brain is shown in purple, Posterior forming spinal cord in yellow, and the somites are shown in green.

**(F)** Heatmap of the expression of the AP domain-associated selected genes in human forebrain, midbrain, hindbrain and spinal cord samples isolated from CS14 human embryos and compared to the Anterior and Posterior NT organoid samples. In the x-axis it is represented the hierarchical clustering of the AP domain-associated genes. In the y-axis it is represented the hierarchical clustering of the samples.

**Figure 3: NT organoids are composed by epithelial polarized cells. (A,B)** Selected images of anterior **(A)** or posterior **(B)** orgaboids stained for the ciliary membrane marker ARL13B (green) and the junctional protein βCatenin (βCAT, magenta). Scale bars = 10

µm. Selected images of the βCAT staining alone are shown in **A'** and **B'**. **(C)** Plots major axis/ minor axis of the cell (aspect ratio) in organoids with mesenchymal-like identity, Anterior, and Posterior organoids (horizontal bold lines show the median; n=100, 100 cells from 5 organoids; ****p<0.0001 Kruskal-Wallis test and Dunn's multiple comparison test). **(D,E)** Selected images of Anterior **(D)** or Posterior **(E)** organoids stained for the centrosome marker pericentrin (PCNT, red) and the junctional complexes protein N-Cadherin (NCAD, blue). Higher magnifications of transversal views are shown in **D'** and **E'**. Scale bars = 10 µm. *En face* views are shown in **D''** and **E''**. Scale bars = 5 µm. **(F)** Plots nuclei to centrosome distance in cells from organoids with mesenchymal identity, Anterior, and Posterior organoids (horizontal bold lines show the median; n=187 cells from 5 organoids; ****p<0.0001 Kruskal-Wallis test and Dunn's multiple comparison test). **(G,H)** Selected images of transversal views of Anterior **(G)** or Posterior **(H)** NT organoids stained for ARL13B (green) and βCAT (magenta). Scale bars = 10 µm. Higher magnifications of mitosis in transversal views are shown in **G'** and **H'**. Scale bars = 5 µm. 3D reconstructions of the apical end foot of the cells are shown in **G''** and **H''**. **(I)** Plots cilia length in cells from organoids with mesenchymal identity, Anterior, and Posterior organoids (horizontal bold lines show the median; n=100, 100 cells from 5 organoids; ****p<0.0001 Kruskal-Wallis test and Dunn's multiple comparison test). **(J,K)** Selected images of transversal views of Anterior **(J)** or Posterior **(K)** organoids stained for the fate-determining factor aPKC (yellow) and the zonular protein ZO1 (cyan). Higher magnifications of transversal views are shown in **J'** and **K'**. Scale bars = 10 µm. 3D reconstructions of the apical surface of the epithelium are shown in **J''** and **K''**. (**J'''** and **K'''**) Plots show the fluorescence intensity to the distance from the organoid lumen (zero). Yellow line represents aPKC, cyan line represents ZO1 and grey line represents DAPI. **(L)** Scheme of polarized neuroepithelial cell in transversal and *en face* views. The centrosome (red) is apically localized. Cilia (green) are nucleated from the centrosomes pointing to the lumen of the tissue (red dots). Apical polarity components are organized in the apical end foot, being aPKC (yellow) apical to ZO1 (cyan) and NCAD (blue). βCAT (magenta) is localized in the cell membrane.

**(M)** Selected images of GFP-expressing posterior organoids, at the beginning and the end of the time-lapse video microscopy, where GFP+ cells are tracked undergoing INM. *In vivo*, organoids are stained for ACTIN (magenta) and GFP (green to blue). Scale bars = 10 µm. **(N)** Plots the cell cycle length estimation from the time-lapses (n=5). **(O)** Zoom in of the sequential time point following a NPC (marked with the red asterisk) undergoing

INM in the organoids showed in **M**. NT organoids are labelled for GFP (green to blue). L= Lumen; M= Matrigel. Scale bars = 10 µm. **(P)** Plot shows the changes in circularity that the NPC undergoes in the time-lapse showed in **O**. Pink areas highlight the mitosis time points. **(Q)** Plots the position of the cell nuclei within the organoid, as the distance to the lumen surface in the time-lapse showed in B. Pink areas highlight the mitosis time points.

**Figure 4: Modelling *de novo* lumen formation in posterior NT organoids and tracking cell intercalation for lumen resolution (A)** Scheme representing the pre-aggregation step protocol for modelling secondary neurulation in posterior NT organoids. The violet square represents the live imaging time window showed in C and D. **(B)** Selected images of the general view of posterior organoids maintained 48h in agitation and then transferred to a Matrigel droplet. **B''** shows a selected image of posterior organoids undergoing multiple lumen formation that spontaneously will later resolve into a single lumen **(B''')**. Organoids are stained for ACTIN (grey), GFP (green) and DAPI (blue). Scale bars = 50 µm.

**(C)** Selected images of the general view of posterior organoids at the beginning and the end of the time-lapse. Organoids are stained for ACTIN (magenta) and GFP (green to blue). Scale bars = 30 µm. **(D)** Zoom in of the sequential time point following a NPCs (marked with the red asterisk) undergoing cell intercalation in the posterior organoids showed in C. Taking the ACTIN staining as reference, a long discontinuous line was drawn to mark the BM while the short discontinuous line represents the apical limit of the epithelia. L= Lumen; M= Matrigel. Scale bars = 10 µm. **(E)** Plot shows the minimum distance of the intercalating cell to the BM showed in D as time goes on. Pink areas highlight the intercalation time points. **(F)** Plots the changes in cell shape assessed by the ratio between major and minor axis of the intercalating cell showed in D as time goes on. Pink areas highlight the intercalation time points.

**Figure 5: Lumen resolution in posterior NT organoids is associated with an increase in cell density and decrease in nuclear YAP. (A)** Selected image of the general view of posterior organoid maintained 48h in agitation and then maintained in a Matrigel droplet for 24h. Scale bars = 20 µm. Zoom in of peripheral and central cells. Scale bars = 5 µm. Organoids are stained for ACTIN (grey), GFP (green) and DAPI (blue). **(A")** Plots the mean area occupied by peripheral and central cells (horizontal bold lines show the

median; n=10, 10 images from 5 organoids; ***p<0.001 Mann-Whitney test**). (B)** Scheme representing central and peripheral cells in relation to cell density. **(C)** Selected images of peripheral and central cells from posterior organoids maintained 48h in agitation and then grown in a Matrigel droplet for 24h. Organoids are stained for ACTIN (grey), YAP (red) and DAPI (blue). Dot line represents the limits of the cells based on the ACTIN staining. Scale bars = 5 µm. **(C‘, C”)** Plots the fluorescence intensity of YAP (red line) to the distance from the organoid lumen (zero) for the central cell and the peripheral cell showed in **C**. Grey boxes represents the limits of the cell based on the ACTIN staining, blue box represents the nuclei localization based on DAPI staining. **(D)** Plots the ratio of the integrated density of the nuclear YAP over the integrated density of YAP in the whole cell (horizontal bold lines show the median; n=23 (peripheral cells) n=18 (central cells), from 7 organoids; *p<0.05 Mann-Whitney test).

**Figure 6: Lumen resolution in posterior NT organoids requires YAP activity.**
**(A)** 3D reconstructions of huNTOrg lumen (ventricle) in control and Dasatinib (DASA) treated cultures. **(B)** Plots the ratio of lumen perimeter mean over the organoid perimeter at day 1, day 2, day 3 and day 4 of culture in control (black) and DASA (orange) (horizontal bold lines show the median; * p<0.05, ** p<0.005, **** p<0.0001, two-way ANOVA).
**(C)** Schematic representation of the culture conditions Pie charts represent the proportion of organoids with single (grey) and multiple (purple) lumen. **(D, E)** Selected images of the general view of posterior organoids maintained 48h in agitation and then transferred to a Matrigel droplet in control conditions **(D)** or with a YAP inhibitor (DASA) (**E**). Organoids are stained for ACTIN (grey), GFP (green) and DAPI (blue). Scale bars = 20 µm. White dot line delimitates the lumen perimeter while, the white discontinuous line delimitates the organoid perimeter. **(F)** Schematic representation of the culture conditions. Pie charts represent the proportion of organoids with single (grey) and multiple (purple) lumen.

## SUPPLEMENTARY FIGURE LEGENDS

**Supplementary Figure S1: Screening for the guidance of hESCs towards NMPs lineage and the subsequent restriction to NPCs in 3D cultures (related to Figure 1).**
**(A)** Plots the quantification of organoids expressing the indicated markers¸ SOX2 (red),

BRA (green) and CDX2 (yellow), after 3, 5 and 7 days in culture. Guiding drugs are indicated at the appropriate days in culture.

**(B)** Selected images of mesenchymal organoids stained for SOX2 (red), BRA (green), and aPKC (grey) at day 3 **(C')**, day 5 **(C'')** and day 7 **(C''')**. **(C-E)** Selected images of NT organoids stained for the indicated markers day 3 **(D')**, day 5 **(D'')** and day 7 **(D''')**. Scale bars = 30 µm.

**Supplementary Figure S2: iPSC generated NT organoids with different anterior-posterior identities (related to Figure 1).**

**(A)** Plots the quantification of organoids expressing the indicated markers¸ SOX2 (red), BRA (green) and CDX2 (yellow), after 3, 5 and 7 days in culture, using CRTD1 and KOLF2C1 iPS cell lines. Guiding drugs are indicated at the appropriate days in culture.

**(B)** Selected images of KOLF2C1 Anterior NT organoids stained for SOX2 (red), BRA (green), aPKC (grey) and CDX2 (yellow) at day 3 **(C')**, day 5 **(C'')** and day 7 **(C''')**. **(D)** Selected images of KOLF2C1 Posterior NT organoids stained for the indicated markers day 3 **(D')**, day 5 **(D'')** and day 7 **(D''')**. Scale bars = 30 µm.

**Supplementary Figure S3: RNAseq of huNTOrg revealed dorsal neural progenitor identities (related to Figure 2).**

**(A)** Diagram of the germinal layer identity-associated genes in the mammalian embryo. Neural lineage (purple-to-yellow), mesodermal lineage (green) and endodermal lineage (grey). **(B)** Heatmap of the of the germinal layer identity-associated genes expression in forebrain, midbrain, hindbrain and spinal cord samples isolated from CS14 human embryos and Anterior and Posterior NT organoids samples.

**(C)** Diagram of the DV domains in the developing NT highlighting the selected genes responsible for the identity of the ventral (p3, pMN, p2-0) and the dorsal (dP6-dP1). **(D)** Heatmap of the expression of the DV domain-associated genes highlighted in **A** in spinal cord samples isolated from CS14 human embryos and Posterior NT organoids samples.

**Supplementary Figure S4: ES cells cultured in the presence of Wnt agonist and FGF were prevented to epithelialize and to self-organize around a lumen (related to Figure 3). (A)** Show schematic representations of the culture conditions used. Pie charts represent the proportion of organoids expressing different levels of SOX2 (red) and BRA (green) for each treatment and timing. **(B)** Selected images of mesenchyme_like

organoids stained for the ciliary membrane marker ARL13B (green), βCAT (magenta), and DAPI (white). Scale bars = 10 µm. Higher magnifications crops are shown. **(C)** Selected images of mesenchyme-like organoids stained for the centrosome marker pericentrin (PCNT, red), the junctional complexes protein N-Cadherin (NCAD, blue), and DAPI (white). Higher magnifications are shown. Scale bars = 10 µm. **(D)** Selected images of mesenchyme organoids stained for the fate-determining factor aPKC (yellow) and ZO1 (cyan). Higher magnifications are shown. Scale bars = 10 µm.

**Supplementary Figure S5: Lumen resolution in the posterior huNTOrg is independent on apoptosis (related to Figure 4).**

**(A)** Schematic representation of the culture conditions Pie charts represent the proportion of organoids with single (grey) and multiple (purple) lumen. **(B)** Selected images of the general view of anterior organoids maintained 48h in agitation and then transferred to a Matrigel droplet, that spontaneously organize a single lumen. Organoids are stained for ACTIN (grey) and DAPI (blue). Scale bars = 50 µm. **(C)** Selected images of the general view of posterior organoids maintained 48h in agitation and then transferred to a Matrigel droplet, that open multiple lumen foci (day 2) that spontaneously organize a single lumen (day 7). Organoids are stained for ACTIN (grey) and DAPI (blue). **(D)** Schematic representation of the culture conditions Pie charts represent the proportion of organoids with single (grey) and multiple (purple) lumen. **(E)** Plots Circularity of the cells (4π area/perimeter) in anterior (A) compared to posterior (P) organoids. As the value approaches 0,0 it indicates increasingly elongated shape. (horizontal bold lines show the median; n=100, 100 cells from 5 organoids; ****p<0.0001 Kruskal-Wallis test and Dunn's multiple comparison test). **(F)** Plots major axis/ minor axis of the cell (aspect ratio) in anterior (A) compared to posterior (P) organoids (horizontal bold lines show the median; n=100, 100 cells from 5 organoids; ****p<0.0001 Kruskal-Wallis test and Dunn's multiple comparison test).

**(G)** Schematic representation of the culture conditions. GFP-expressing posterior organoids were maintained 48h in agitation and then transferred to a Matrigel droplet and fixed after 24h for staining. **(H)** Selected image of posterior organoids stained with Phalloidin (grey), Caspase3 (red), GFP (green) and DAPI (blue). Scale bars = 10 µm. **(I)** Plot shows the percentage of Caspase positive cells in central vs peripheral cells. Horizontal bold lines show the median; n=8 organoids; son significant differences. Mann-Whitney test**.**

# REFERENCES


1. Tzouanacou, E., Wegener, A., Wymeersch, F. J., Wilson, V. & Nicolas, J. F. Redefining the progression of lineage segregations during mammalian embryogenesis by clonal analysis. *Dev Cell* **17**, 365–376 (2009).

2. Henrique, D., Abranches, E., Verrier, L. & Storey, K. G. Neuromesodermal progenitors and the making of the spinal cord. *Development* **142**, 2864–2875 (2015).

3. Gouti, M. *et al.* A Gene Regulatory Network Balances Neural and Mesoderm Specification during Vertebrate Trunk Development. *Dev Cell* **41**, 243—-261 e7 (2017).

4. Gouti, M., Metzis, V. & Briscoe, J. The route to spinal cord cell types: a tale of signals and switches. *Trends Genet* **31**, 282–289 (2015).

5. Murielle Saade and Elisa Martí. Early Spinal Cord Development: From Neural Tube Formation to Neurogenesis Mechanisms. *Nature review Neuroscience; (under review; ref: NRN-23-294S)*.

6. Santos, C. *et al.* Spinal neural tube formation and regression in human embryos. *Elife* **12**, (2023).

7. Saitsu, H., Yamada, S., Uwabe, C., Ishibashi, M. & Shiota, K. Development of the posterior neural tube in human embryos. *Anat Embryol (Berl)* **209**, 107–117 (2004).

8. Saitsu, H. & Shiota, K. Involvement of the axially condensed tail bud mesenchyme in normal and abnormal human posterior neural tube development. *Congenit Anom (Kyoto)* **48**, 1–6 (2008).

9. O'Rahilly, R. & Müller, F. Stages in Early Human Development. *Future Aspects in Human In Vitro Fertilization* 238–244 (1987) doi:10.1007/978-3-642-71412-2_33.

10. Gonzalez-Gobartt, E. *et al.* Cell intercalation driven by SMAD3 underlies secondary neural tube formation. *Dev Cell* **56**, 1147–1163.e6 (2021).

11. Blom, H. J., Shaw, G. M., Den Heijer, M. & Finnell, R. H. Neural tube defects and folate: case far from closed. *Nature Reviews Neuroscience 2006 7:9* **7**, 724–731 (2006).

12. Greene, N. D. & Copp, A. J. Neural tube defects. *Annu Rev Neurosci* **37**, 221–242 (2014).

13. Uzquiano, A. & Arlotta, P. Brain organoids: the quest to decipher human-specific features of brain development. *Curr Opin Genet Dev* **75**, 101955 (2022).

14. Karzbrun, E. *et al.* Human neural tube morphogenesis in vitro by geometric constraints. *Nature* **599**, 268–272 (2021).

15. Park, J. S., Hsiung, H. A., Khven, I., Manno, G. La & Lutolf, M. P. Self-organizing in vitro mouse neural tube organoids mimic embryonic development. *Development (Cambridge)* **149**, (2022).

16. Duval, N. *et al.* Bmp4 patterns smad activity and generates stereotyped cell fate organization in spinal organoids. *Development (Cambridge)* **146**, (2019).

17. Meinhardt, A. *et al.* 3D reconstitution of the patterned neural tube from embryonic stem cells. *Stem Cell Reports* **3**, 987–999 (2014).

782 18. Ranga, A. *et al.* Neural tube morphogenesis in synthetic 3D microenvironments. *Proc*
783 *Natl Acad Sci U S A* **113**, E6831–E6839 (2016).

784 19. Zheng, Y. *et al.* Dorsal-ventral patterned neural cyst from human pluripotent stem cells
785 in a neurogenic niche. *Sci Adv* **5**, 1–14 (2019).

786 20. Ogura, T., Sakaguchi, H., Miyamoto, S. & Takahashi, J. Three-dimensional induction of
787 dorsal, intermediate and ventral spinal cord tissues from human pluripotent stem cells.
788 *Development (Cambridge)* **145**, (2018).

789 21. Libby, A. R. G. *et al.* Axial elongation of caudalized human organoids mimics aspects of
790 neural tube development. *Development (Cambridge)* **148**, (2021).

791 22. Rifes, P. *et al.* Modeling neural tube development by differentiation of human
792 embryonic stem cells in a microfluidic WNT gradient. *Nat Biotechnol* **38**, 1265–1273
793 (2020).

794 23. Tang, C., Wang, X., D'Urso, M., van der Putten, C. & Kurniawan, N. A. 3D Interfacial and
795 Spatiotemporal Regulation of Human Neuroepithelial Organoids. *Advanced Science* **9**,
796 2201106 (2022).

797 24. Simunovic, M. *et al.* A 3D model of a human epiblast reveals BMP4-driven symmetry
798 breaking. *Nature Cell Biology 2019 21:7* **21**, 900–910 (2019).

799 25. Turner, D. A. *et al.* Anteroposterior polarity and elongation in the absence of
800 extraembryonic tissues and of spatially localised signalling in gastruloids: Mammalian
801 embryonic organoids. *Development (Cambridge)* **144**, 3894–3906 (2017).

802 26. Olivera-Martinez, I., Harada, H., Halley, P. A. & Storey, K. G. Loss of FGF-Dependent
803 Mesoderm Identity and Rise of Endogenous Retinoid Signalling Determine Cessation of
804 Body Axis Elongation. *PLoS Biol* **10**, e1001415 (2012).

805 27. Ribes, V., Le Roux, I., Rhinn, M., Schuhbaur, B. & Dollé, P. Early mouse caudal
806 development relies on crosstalk between retinoic acid,Shh and Fgf signalling pathways.
807 *Development* **136**, 665–676 (2009).

808 28. Wilson, V., Olivera-Martinez, I. & Storey, K. G. Stem cells, signals and vertebrate body
809 axis extension. *Development* **136**, 1591–1604 (2009).

810 29. Wilson, P. A. & Hemmati-Brivanlou, A. Induction of epidermis and inhibition of neural
811 fate by Bmp-4. *Nature* **376**, 331–333 (1995).

812 30. Chambers, S. M. *et al.* Highly efficient neural conversion of human ES and iPS cells by
813 dual inhibition of SMAD signaling. *Nat Biotechnol* **27**, 275–280 (2009).

814 31. Verrier, L., Davidson, L., Gierlinśki, M., Dady, A. & Storey, K. G. Neural differentiation,
815 selection and transcriptomic profiling of human neuromesodermal progenitor-like cells
816 in vitro. *Development (Cambridge)* **145**, (2018).

817 32. Haremaki, T. *et al.* Self-organizing neuruloids model developmental aspects of
818 Huntington's disease in the ectodermal compartment. *Nat Biotechnol* **37**, 1198–1208
819 (2019).

820 33. Olivera-Martinez, I. & Storey, K. G. Wnt signals provide a timing mechanism for the FGF-
821 retinoid differentiation switch during vertebrate body axis extension. *Development* **134**,
822 2125–2135 (2007).

823 34. Takemoto, T., Uchikawa, M., Kamachi, Y. & Kondoh, H. Convergence of Wnt and FGF
824 signals in the genesis of posterior neural plate through activation of the Sox2 enhancer
825 N-1. *Development* **133**, 297–306 (2006).

826 35. Edri, S., Hayward, P., Jawaid, W. & Arias, A. M. Neuro-mesodermal progenitors (NMPs):
827 A comparative study between pluripotent stem cells and embryo-derived populations.
828 *Development (Cambridge)* **146**, (2019).

829 36. Koch, F. *et al.* Antagonistic Activities of Sox2 and Brachyury Control the Fate Choice of
830 Neuro-Mesodermal Progenitors. *Dev Cell* **42**, 514—-526 e7 (2017).

831 37. del Corral, R. D. *et al.* Opposing FGF and Retinoid Pathways Control Ventral Neural
832 Pattern, Neuronal Differentiation, and Segmentation during Body Axis Extension.
833 *Neuron* **40**, 65–79 (2003).

834 38. Metzis, V. *et al.* Nervous System Regionalization Entails Axial Allocation before Neural
835 Differentiation. *Cell* **175**, 1105–1118.e17 (2018).

836 39. Rayon, T., Maizels, R. J., Barrington, C. & Briscoe, J. Single-cell transcriptome profiling of
837 the human developing spinal cord reveals a conserved genetic programme with human-
838 specific features. *Development (Cambridge)* **148**, (2021).

839 40. Holland, L. Z. *et al.* Evolution of bilaterian central nervous systems: A single origin?
840 *Evodevo* **4**, 1–20 (2013).

841 41. Akin, Z. N. & Nazarali, A. J. Hox genes and their candidate downstream targets in the
842 developing central nervous system. *Cell Mol Neurobiol* **25**, 697–741 (2005).

843 42. Porter, F. D. *et al.* Lhx2, a LIM homeobox gene, is required for eye, forebrain, and
844 definitive erythrocyte development. *Development* **124**, 2935–2944 (1997).

845 43. Yan, C. H., Levesque, M., Claxton, S., Johnson, R. L. & Ang, S. L. Lmx1a and Lmx1b
846 function cooperatively to regulate proliferation, specification, and differentiation of
847 midbrain dopaminergic progenitors. *Journal of Neuroscience* **31**, 12413–12425 (2011).

848 44. Kumamoto, T. & Hanashima, C. Evolutionary conservation and conversion of Foxg1
849 function in brain development. *Dev Growth Differ* **59**, 258–269 (2017).

850 45. Basson, M. A. *et al.* Erratum: Specific regions within the embryonic midbrain and
851 cerebellum require different levels of FGF signaling during development (Development
852 vol. 135 (889-898)). *Development* **136**, 1962 (2009).

853 46. Deng, Q. *et al.* Specific and integrated roles of Lmx1a, Lmx1b and Phox2a in ventral
854 midbrain development. *Development* **138**, 3399–3408 (2011).

855 47. de Vries, M. *et al.* Interrogating the Grainyhead-like 2 (Grhl2) genomic locus identifies
856 an enhancer element that regulates palatogenesis in mouse. *Dev Biol* **459**, 194–203
857 (2020).

858 48. Pani, A. M. *et al.* Ancient deuterostome origins of vertebrate brain signalling centres.
859 *Nature* **483**, 289–294 (2012).

860 49. Hirata, H. Hes1 and Hes3 regulate maintenance of the isthmic organizer and
861 development of the mid/hindbrain. *EMBO J* **20**, 4454–4466 (2001).

862 50. Alaynick, W. A., Jessell, T. M. & Pfaff, S. L. SnapShot: Spinal cord development. *Cell* **146**,
863 178.e1–178.e1 (2011).

864 51. Saade, M., Blanco-Ameijeiras, J., Gonzalez-Gobartt, E. & Martí, E. A centrosomal view of
865 CNS growth. *Development* **145**, (2018).

866 52. Blanco-Ameijeiras, J., Lozano-Fernández, P. & Martı, E. Centrosome maturation – in
867 tune with the cell cycle. *J Cell Sci* **135**, (2022).

868 53. Paridaen, J. T., Wilsch-Brauninger, M. & Huttner, W. B. Asymmetric inheritance of
869 centrosome-associated primary cilium membrane directs ciliogenesis after cell division.
870 *Cell* **155**, 333–344 (2013).

871 54. Saade, M., Gonzalez-Gobartt, E., Escalona, R., Usieto, S. & Marti, E. Shh-mediated
872 centrosomal recruitment of PKA promotes symmetric proliferative neuroepithelial cell
873 division. *Nat Cell Biol* **19**, 493–503 (2017).

874 55. Saade, M. *et al.* Multimerization of Zika Virus-NS5 Causes Ciliopathy and Forces
875 Premature Neurogenesis. *Cell Stem Cell* **27**, 920–936.e8 (2020).

876 56. Afonso, C. & Henrique, D. PAR3 acts as a molecular organizer to define the apical
877 domain of chick neuroepithelial cells. *J Cell Sci* **119**, 4293–4304 (2006).

878 57. Aaku-Saraste, E., Hellwig, A. & Huttner, W. B. Loss of occludin and functional tight
879 junctions, but not ZO-1, during neural tube closure–remodeling of the neuroepithelium
880 prior to neurogenesis. *Dev Biol* **180**, 664–679 (1996).

881 58. Marthiens, V. & Ffrench-Constant, C. Adherens junction domains are split by
882 asymmetric division of embryonic neural stem cells. *EMBO Rep* **10**, 515–520 (2009).

883 59. Chenn, A., Zhang, Y. A., Chang, B. T. & McConnell, S. K. Intrinsic polarity of mammalian
884 neuroepithelial cells. *Mol Cell Neurosci* **11**, 183–193 (1998).

885 60. Sauer, F. C. Mitosis in the neural tube. *Journal of Comparative Neurology* **62**, 377–405
886 (1935).

887 61. Morris, J. K. *et al.* Prevention of neural tube defects in the UK: a missed opportunity.
888 *Arch Dis Child* **101**, 604–607 (2016).

889 62. Elosegui-Artola, A. *et al.* Force Triggers YAP Nuclear Entry by Regulating Transport
890 across Nuclear Pores. *Cell* **171**, 1397–1410.e14 (2017).

891 63. Nardone, G. *et al.* YAP regulates cell mechanics by controlling focal adhesion assembly.
892 *Nat Commun* **8**, (2017).

893 64. Varelas, X. *et al.* TAZ controls Smad nucleocytoplasmic shuttling and regulates human
894 embryonic stem-cell self-renewal. *Nat Cell Biol* **10**, 837–848 (2008).

895 65. Varelas, X. *et al.* The Crumbs Complex Couples Cell Density Sensing to Hippo-Dependent
896 Control of the TGF-β-SMAD Pathway. *Dev Cell* **19**, 831–844 (2010).

897 66. Hsu, P. C., Yang, C. T., Jablons, D. M. & You, L. The role of yes-associated protein (YAP)
898 in regulating programmed death-ligand 1 (PD-L1) in thoracic cancer. *Biomedicines* **6**, 1–
899 10 (2018).

900 67. Wolujewicz, P. *et al.* Genome-wide investigation identifies a rare copy-number variant
901 burden associated with human spina bifida. *Genetics in Medicine* **23**, 1211–1218 (2021).

902 68. Vong, K. I. *et al.* Risk of meningomyelocele mediated by the common 22q11.2 deletion.
903 *Science (1979)* **384**, 584–590 (2024).

904 69. Lei, Y.-P. *et al.* VANGL2 Mutations in Human Cranial Neural-Tube Defects . *New England*
905 *Journal of Medicine* **362**, 2232–2235 (2010).

906 70. Kibar, Z. *et al.* Mutations in VANGL1 Associated with Neural-Tube Defects. *New England*
907 *Journal of Medicine* **356**, 1432–1437 (2007).

908 71. Piccolo, S., Dupont, S. & Cordenonsi, M. The biology of YAP/TAZ: Hippo signaling and
909 beyond. *Physiol Rev* (2014) doi:10.1152/physrev.00005.2014.

910

Blanco-Ameijeiras, Figure 1

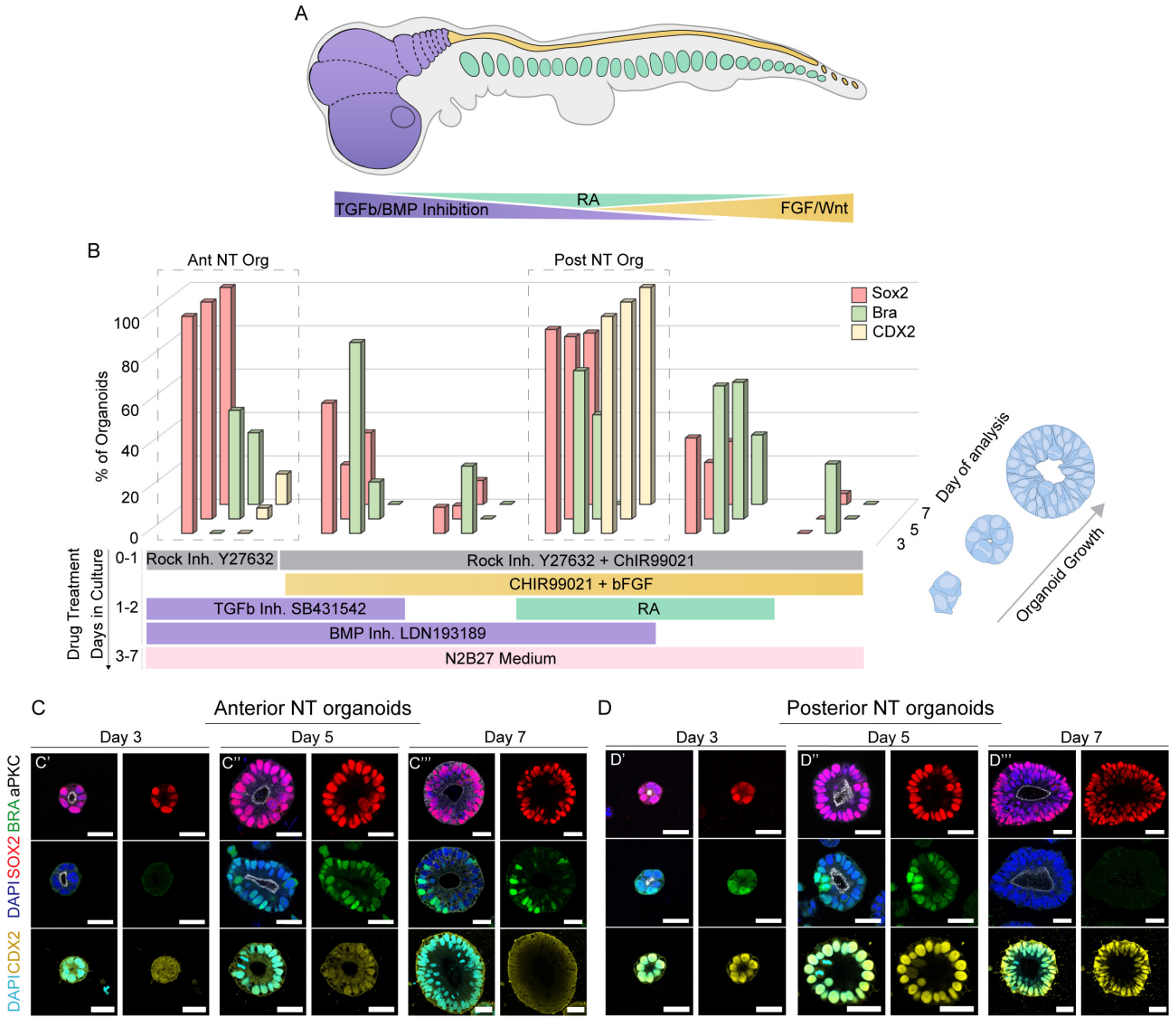

Blanco-Ameijeiras, Figure 2

A

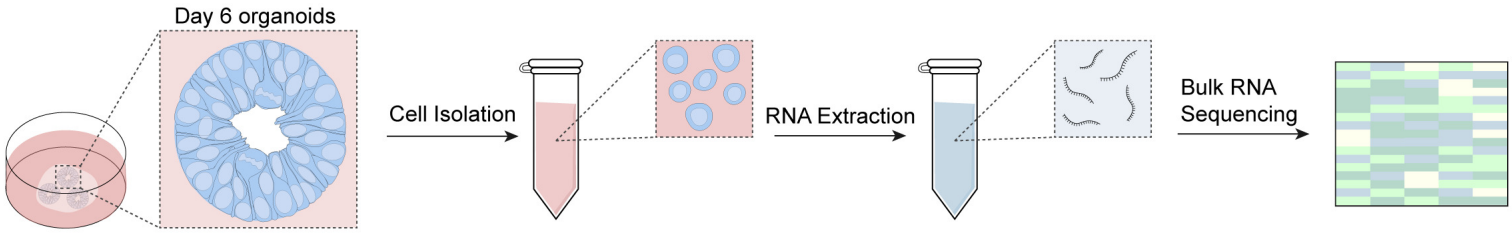


B

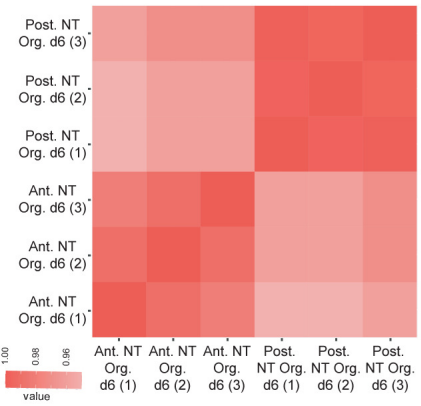


C

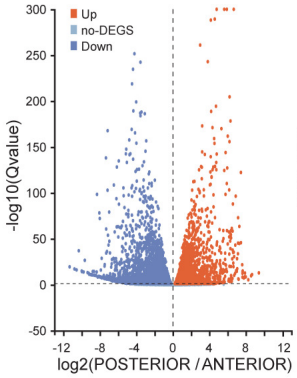


D

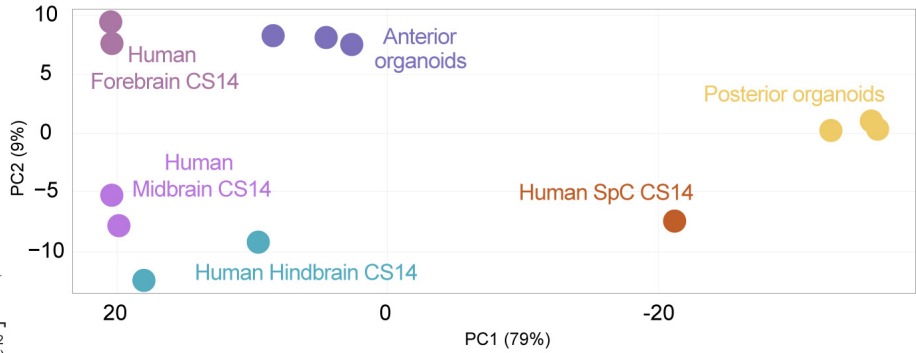


E

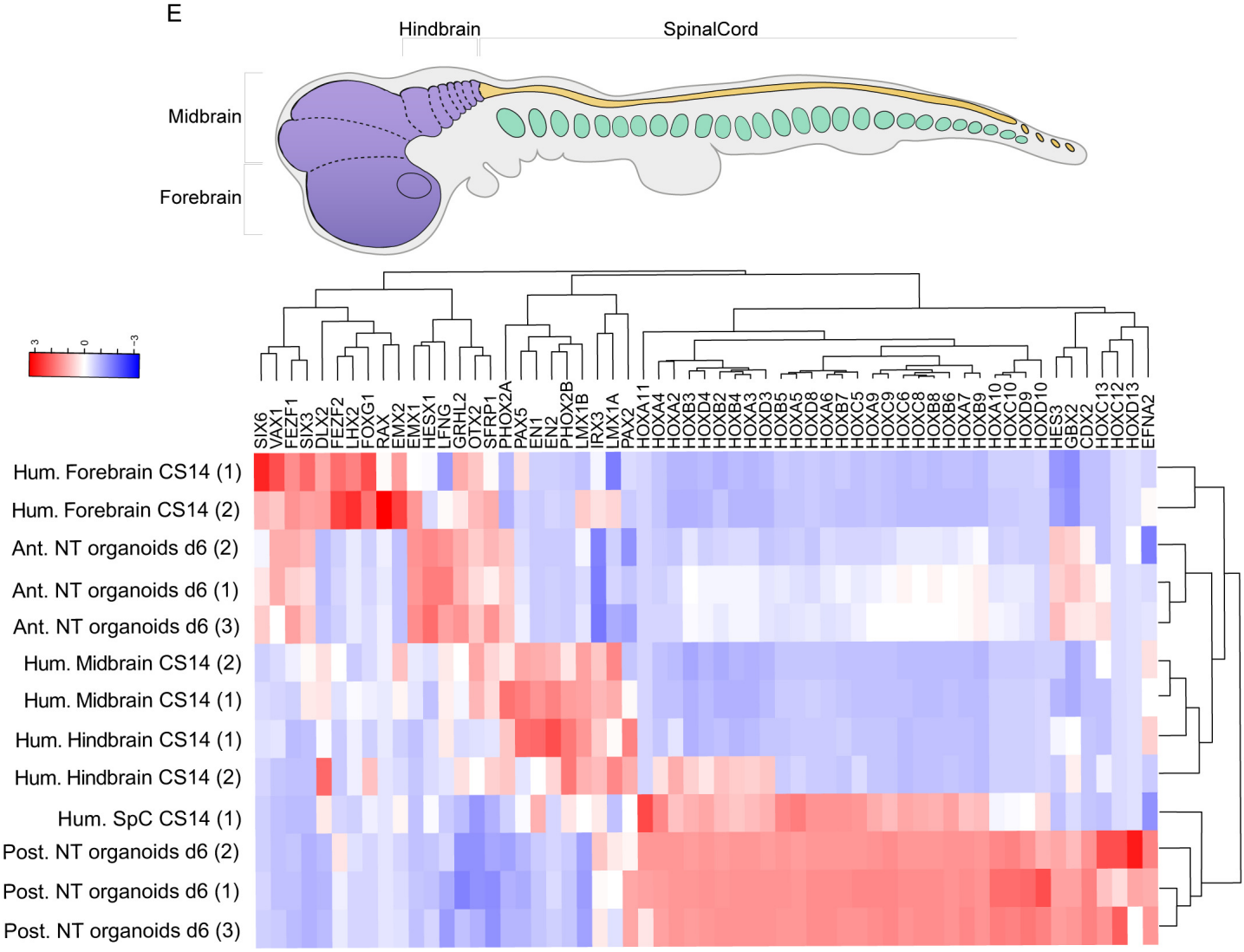

Blanco-Ameijeiras, Figure 3

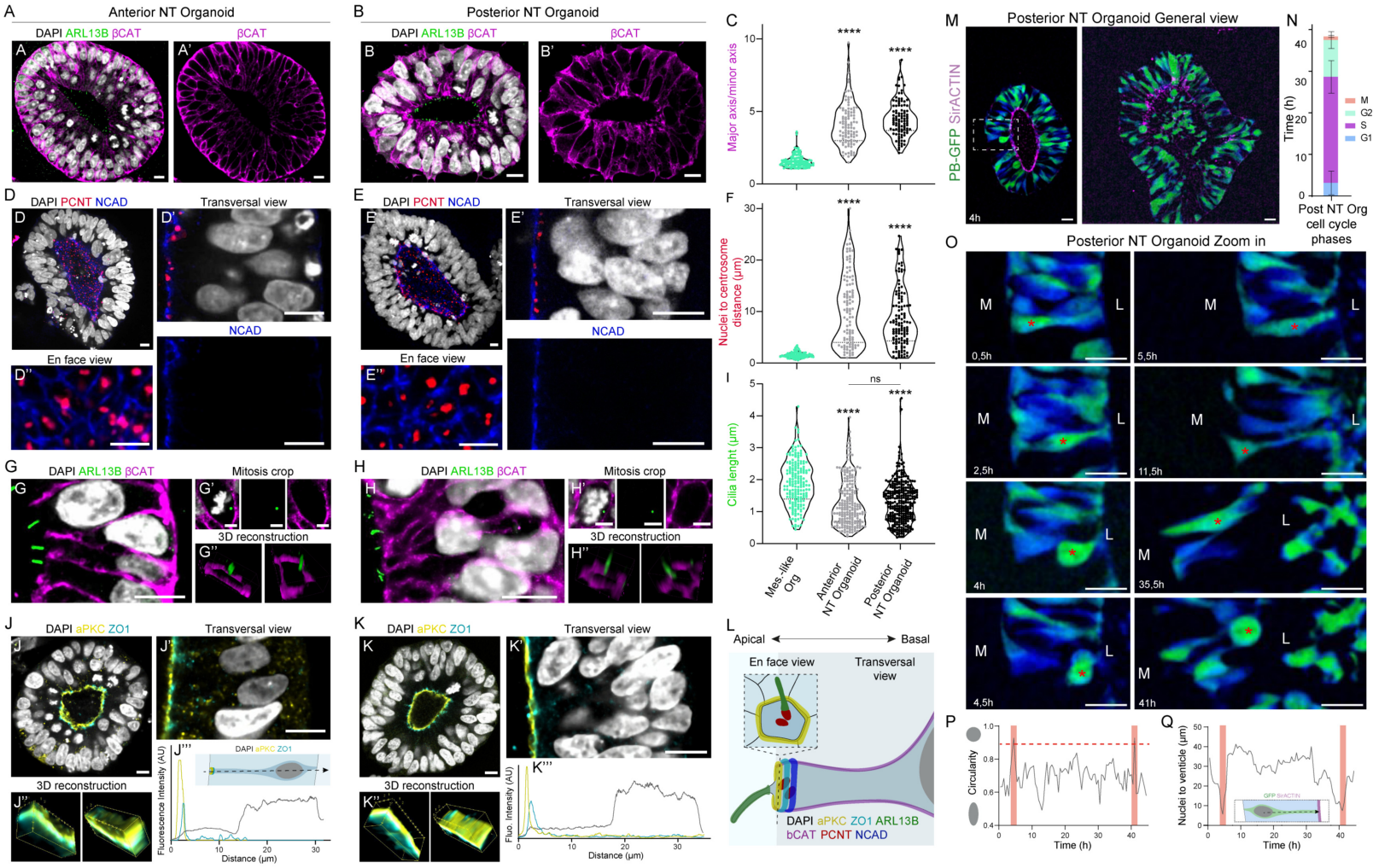

Blanco-Ameijeiras, Figure 4

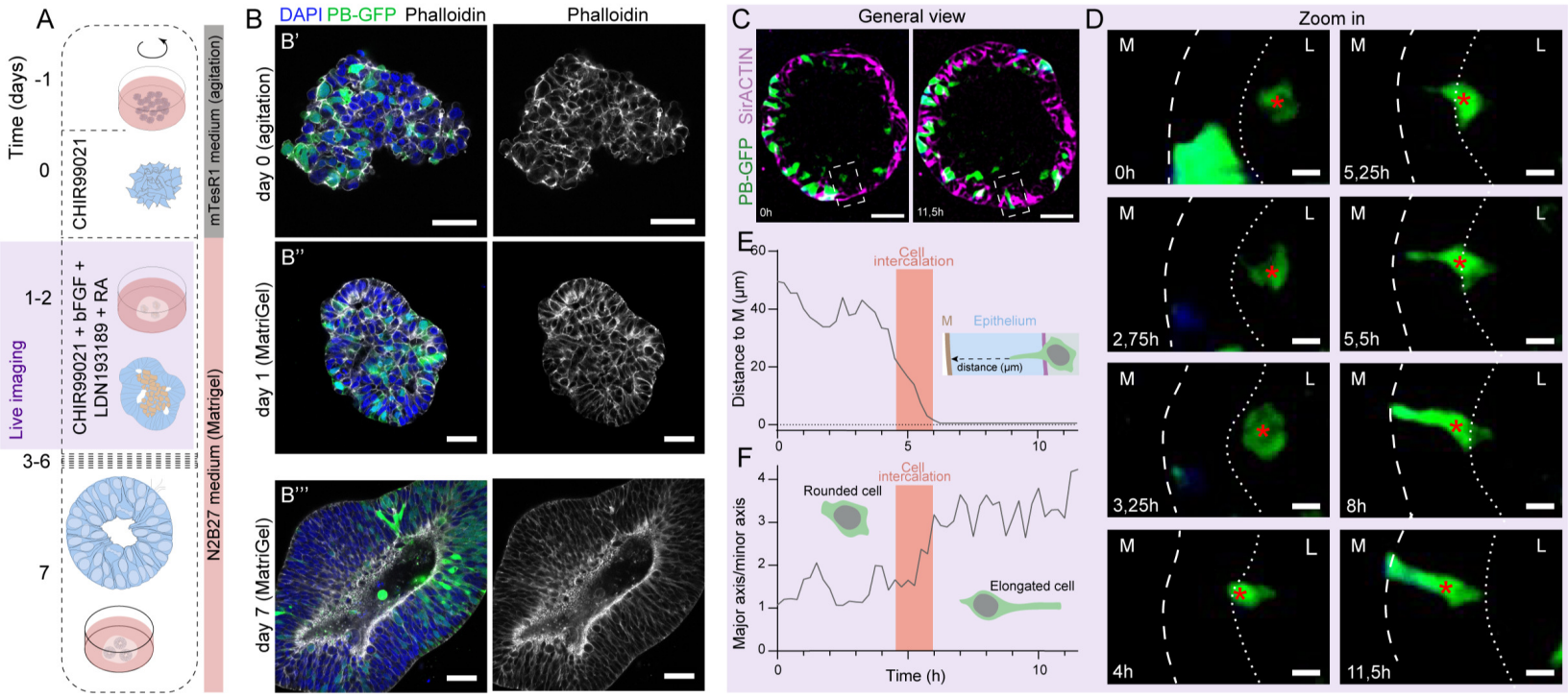

Blanco-Ameijeiras, Figure 5

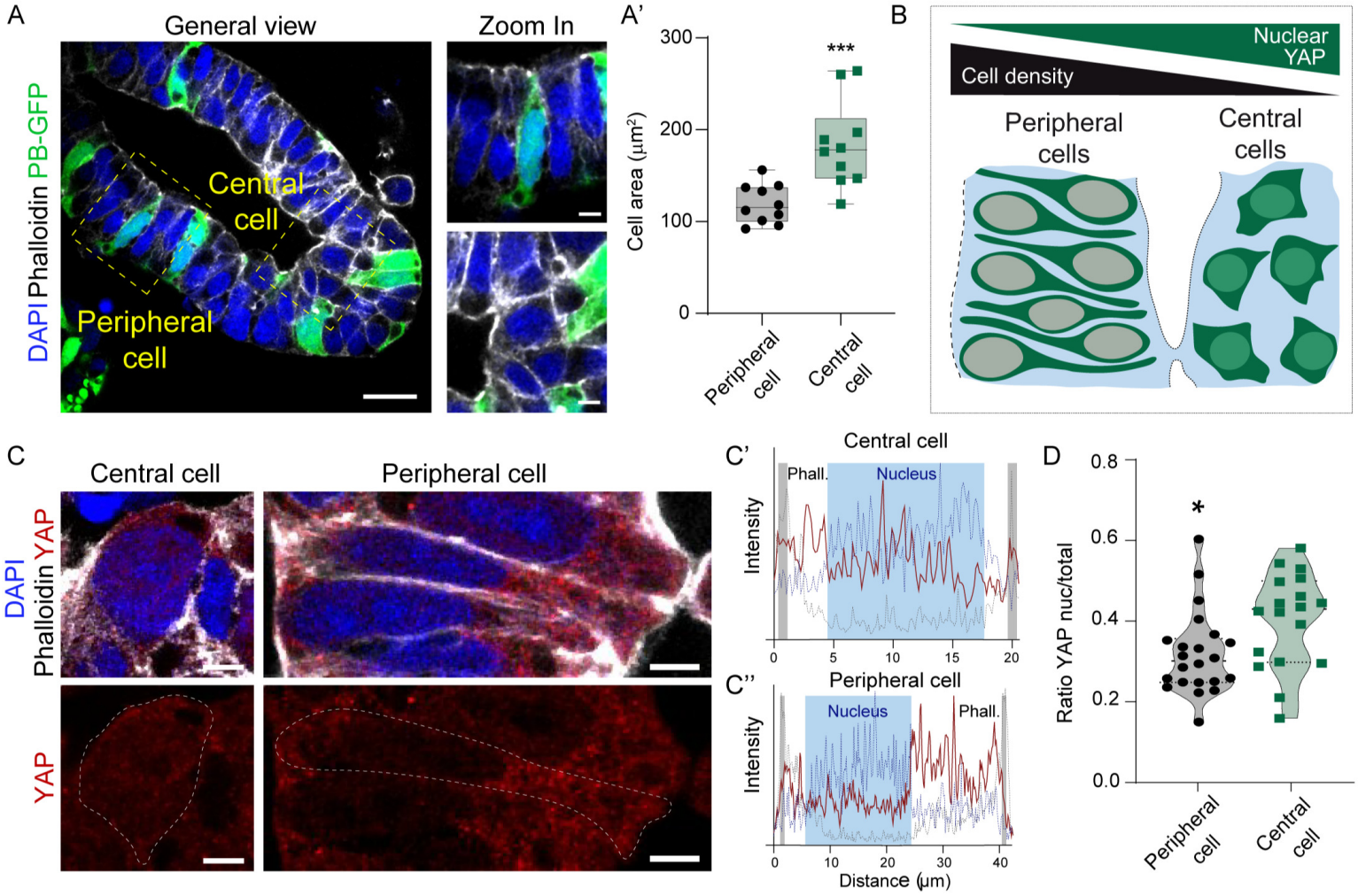
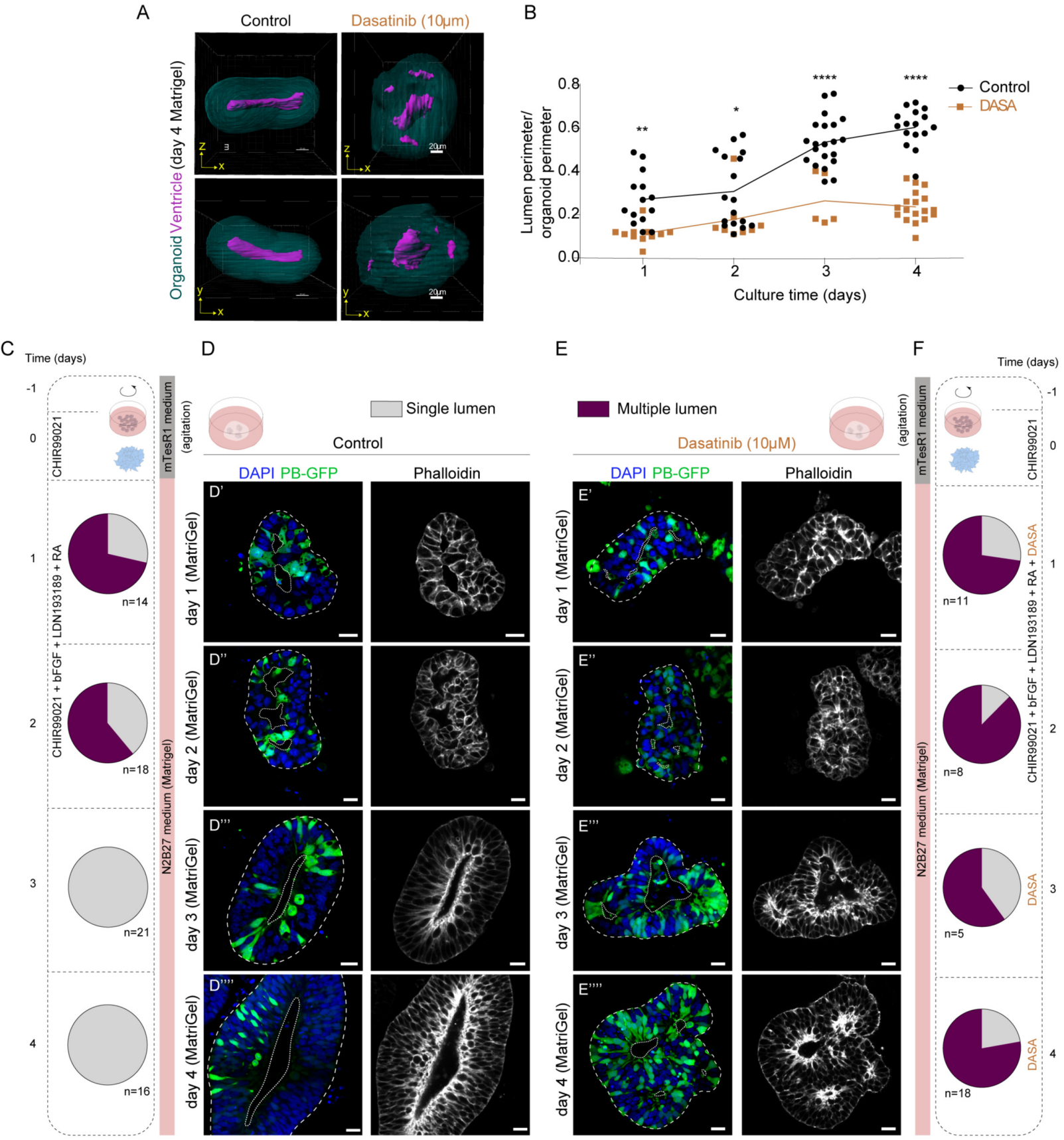
Blanco-Ameijeiras, Figure 6